

INFLUENCE OF POST-DEPOSITION ANNEALING ON THE INDIUM TIN OXIDE THIN FILMS GROWN BY PULSED LASER DEPOSITION

N. MUSTAPHA^{a,*}, A. ALAKHRAS^b, H. IDRIS^{c,d}

^a*Department of Physics, College of Science, Imam Mohammad Ibn Saud Islamic University, P.O. Box 90950, Riyadh 11623, Saudi Arabia*

^b*Department of Chemistry, College of Science, Imam Mohammad Ibn Saud Islamic University, P.O. Box 90950, Riyadh 11623, Saudi Arabia*

^c*Deanship of scientific research, College of Science, Imam Mohammad Ibn Saud Islamic University, Saudi Arabia*

^d*Sudan Atomic Energy Commission*

Transparent thin-film Indium Tin Oxides (ITO) were prepared on glass substrates using a pulsed laser deposition (PLD) process with an average thickness of 150 nm. Post-deposition annealing was performed on the samples in a wide range of temperatures from 250 to 650 °C. The surface structures of as-deposited and annealed ITO films were analyzed using the x-ray diffraction (XRD). Atomic Force Microscopy (AFM) was carried out on all samples to verify any change in the grain sizes, and in the roughness of the oxide thin film surfaces. The transmittance spectra of the annealed samples were also investigated using spectrophotometer measurements. Energy band gaps E_g were calculated from the optical spectra for all films. It was found that the optical band gap values decreased as the annealing temperature was increased. To compare the effect of the annealing on refractive index n and extinction coefficient k properties, additional measurements were done on the samples pre and post annealing using an ellipsometer. It is noted that the annealed ITO films resulted in a noticeable improvement in the crystalline structure and an increase in the surface roughness. Furthermore, their maintained good optical properties made them very favorable to be used in different disciplines such as anodes of the solar cells and as protective coatings in space windows.

(Received August 23, 2020; Accepted December 17, 2020)

Keywords: Indium tin oxide, Pulsed laser deposition, Atomic force microscopy, X-ray diffraction, Optical properties

1. Introduction

Indium Tin oxide (ITO) thin films are widely used as transparent conductive oxide (TCO) films because of their excellent optoelectronic characteristics. They are electrically conductive materials with comparably low absorption of light. This material observed high transmittance (> 75%) in the visible region as well as a band-gap around 3.2 eV. Thin films can be obtained using different processes such as chemical vapor deposition (CVD), sputtering sol-gel, atomic layer deposition and pulsed laser deposition (PLD) [1-5]. (TCO's) have been widely used in solar cells, light emitted diodes (LEDs), Thin Film Transistor (TFTs), liquid crystal displays and smart windows [5-9].

An indium tin oxide is a compound which consists of indium, tin, and oxygen in varying proportions. Usually, ITO in thin-film form is colorless and transparent. In contrast, in bulk form its color is yellow-gray. ITO is mainly deposited by Physical Vapor deposition (PVD). The thin films (100–300nm) with a cubic crystal structure and a lattice constant ($a = 1.0117$ nm) exhibited a wide range of band-gaps from 3.3 to 4.3 eV and low sheet resistance of 20 Ω /sq. In addition, the film's transmittance became greater than 80% in the visible region [9].

* Corresponding author: nazirmustapha@yahoo.co.uk

The importance of oxide films in the optoelectronic devices made them the focus of investigation by many researchers. DC sputtering process resulted in a highly conductive and transparent ITO film with a thickness of 350 nm a resistivity of $6.85 \times 10^{-4} \Omega \text{ cm}$ and transmittance of 88% [13]. On the other hand, the PLD process showed a thin film of ITO with a polycrystalline structure and a resistivity of $1.1 \times 10^{-3} \Omega \cdot \text{cm}$ and transmittance of 92% [3]. In general, the properties of TCO thin films depend on many factors such as deposition method and parameters. In addition, the substrate temperature, ambient atmosphere play important roles in the optical and electrical properties of the thin film as well as the microstructure of the films [3, 4].

There are many published papers to investigate the structural, morphological, electrical and optical properties of ITO thin films deposited by magnetron sputtering [10-13].

However, there are few studies to explore the effects of post-deposition annealing on the optical, structural and morphological properties of ITO deposited by pulsed laser deposition.

The aim of this research was to deposit (ITO) thin films onto glass substrates using a high purity target of 99.995% and by using pulsed laser deposition technique. The optical, morphological and structural characterization of deposited thin film layers (150- 180 nm thick) were investigated. A range of post-deposition annealing temperatures (250-650 °C) was used to assess its influence on film optical, structural and morphological properties.

2. Experimental procedure

2.1. Thin film deposition

Indium oxide (In_2O_3) and tin oxide (SnO_2) were purchased from the American Dye Source (ADS) company and the purities were 99.995 and 99.998%, respectively and used as received. The indium Tin Oxide (ITO) pellets were synthesized using 90% of In_2O_3 with 10% of SnO_2 . Glass substrates were used for the deposition of the oxide films.

Prior to the deposition of ITO films, each glass substrate was cleaned with acetone, methanol and washed thoroughly in deionized water using an ultrasonic bath. The glass substrates were also dried using high purity nitrogen. In the final cleaning step, the substrates were dried in furnace at 120 °C for a duration of 30 minutes. Then, the substrates were loaded into the deposition chamber. The target and substrate distance was kept at 15 cm for all depositions.

A KrF excimer laser source with a wavelength of 248 nm and a laser repetition rate of 10 Hz was used inside PLD/MBE 2100 from PVD Products growth chamber to deposit ITO films onto glass substrates at a base pressure of 10^{-6} Torr under oxygen pressure and temperature of 10 mTorr and 300 °C, respectively. PLD system produces high-quality films with dimensions of 1.5 cm \times 1.5 cm substrate area and a thickness of 150 nm in an average variation of less than 10% for each sample used [3]. Eventually, Deck Tack 150 was used to assess the film thickness.

2.2. Annealing

Deposited films were annealed using furnace (CARBOLITE CWF-1200). For this study, annealing of ITO thin films was performed at different temperatures (250, 350, 450, 550 and 650) °C for 2 hours in air, and then characterized in order to investigate the changes in morphology, structure and optical properties if any.

2.3. X-Ray measurement

The as-deposited and post-annealed TCO films were subjected to X-ray diffraction (XRD) using Bruker-AXS D8 ADVANCE X-ray diffractometer with $\text{CuK}_{\alpha 1}$ radiation, the typical high voltage current were 45kV and 30 mA respectively.

Copper $\text{K}\alpha$ x-rays of wavelength 1.54 \AA were used for the diffraction. At the angle θ the X-ray beam is incident on the parallel planes of atom, either constructively or destructively the waves react due to path difference. Bragg's law describes the condition on θ for the constructive interference for Scattered X-rays at its strongest according to the following equation:

$$2d_{hkl} \sin\theta = n\lambda \quad (1)$$

where: d , θ , n and λ are the inter-planar spacing of the crystal lattice, Bragg's angle, an integer representing the order of the diffraction peak, and the wavelength of hitting X-ray beam, respectively. Furthermore, h , k and l are the Miller indices of the crystallographic planes. Grain size (D) is calculated using the Scherrer equation, such as:

$$D = \frac{\kappa\lambda}{\beta \cdot \cos \theta} \quad (2)$$

where λ the wavelength of Cu K α radiation, $k = 0.9$, β is the full width at half maximum of the diffraction peak (FWHM) and θ is the Bragg angle.

2.4. Atomic Force Microscopy scanning

The morphology and surface roughness of freshly deposited samples (to avoid the effects of humidity) were investigated using Atomic Force Microscopy (AFM) Multi-Mode8-Bruker.

2.5. UV-visible Spectrometer measurement

The optical properties such as transmission and absorption of the oxide films deposited on glass substrates were measured using a Perkin Elmer Lambda 950 UV-VIS spectrophotometer over the range from 300 to ~ 800 nm.

2.6. Ellipsometer measurement

The optical constants such as refractive index (n) and extinction coefficient (k) for each sample were measured using an Ellipsometer Spectroscopy (ES) (UVISEL, from HORIBA).

3. Results and discussions

3.1. Effect of annealing on the structural properties of ITO films

XRD patterns of ITO are shown in Fig. 1, which suggest that the films are of polycrystalline nature. Diffraction peaks at 2θ of 21.4° , 30.6° , 35.4° , 51.0° and 60.6° correspond to cubic ITO (211), (222), (400), (440) and (622), respectively. No other diffraction peak is detected, which means that all six samples are ITO. The peak shift to the right which means an increase in crystal lattice. Through the annealing process, we get a set order of the atoms, which mean it will be more crystalline, attributed to increase in the intensity of the peak. According to D'Elia and co-authors the improvement in the crystalline structure of the ITO thin films was due to the oxygen absorption during annealing in air [14].

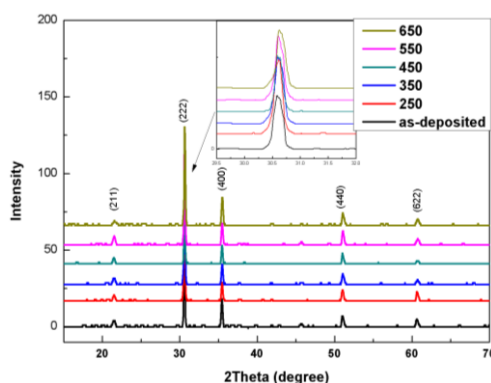


Fig. 1. XRD patterns of ITO thin films deposited on glass, annealed at 250, 350, 450, 550, and 650 °C

Lattice constant was calculated using Plane-Spacing equation:

$$d_{hkl} = \frac{a}{\sqrt{h^2+k^2+l^2}} \quad (3)$$

The values of 2θ , d and a for the (222) peak of the as-deposited and annealed ITO thin films are represented in Table 1.

Table 1. The values of 2θ , d and a for the (222) peak of the as-deposited and annealed ITO thin films.

T(°C)	2θ(degree)	d(Å)	a (nm)
As – deposited	30.58	1.89	0.65
250	30.61	1.96	0.68
350	30.62	1.98	0.69
450	30.61	1.96	0.68
550	30.63	2.01	0.70
650	30.65	2.06	0.71

Grain size can be calculated using equation (2) with a wavelength of the X-ray sources $\lambda = 1.54$ nm. Table 2 shows the average grain size of the as-deposited and annealed ITO thin films.

From Table 2, we noticed that the FWHM decreased after annealing which was a sign of an increase in grain size.

Table 2. Average grain size of the as-deposited and annealed ITO thin films.

T(°C)	β(rad)	θ(degree)	Cos θ	D (nm)
As – deposited	3.8×10^{-3}	15.29	0.96	37.81
250	3.4×10^{-3}	15.30	0.96	42.26
350	3.3×10^{-3}	15.31	0.96	43.54
450	2.9×10^{-3}	15.30	0.96	49.55
550	2.7×10^{-3}	15.31	0.96	53.21
650	2.6×10^{-3}	15.32	0.96	55.26

A considerable increase in average grain size from 43 nm to 49 nm is found between 350 °C and 450 °C temperature, increase in lattice constant from 0.65 nm to 0.68 nm is found after annealing at 250 °C as shown in Fig. 2. The results represented in Table 1, by using Sherrer equation, showed that the ITO samples (38-55nm) become more crystalline above 550 °C annealing Temperature.

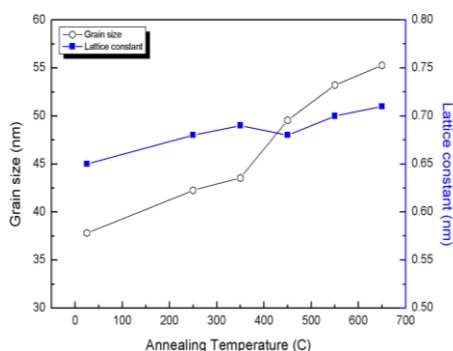


Fig. 2. Grain size and Lattice constant of ITO change with Annealing Temperature.

Table 3 represents the values of 2θ , d and a for (100) peak of the as-deposited and annealed ITO thin films.

Table 3. The values of 2θ , d and a for (100) peak of the as-deposited and annealed ITO thin films.

T ($^{\circ}\text{C}$)	2θ (degree)	d (\AA)	a (nm)
As – deposited	33.31	2.68	0.65
250	33.93	2.63	0.68
350	34.15	2.62	0.69
450	34.30	2.61	0.68
550	34.32	2.60	0.70
650	34.34	2.60	0.71

3.2 Effect of annealing on the morphological properties of ITO

Figs. 3 and 4 illustrate the AFM three-dimensional view of film morphology of ITO and two-dimensional view of surface morphology, respectively. We can observe from figure (4a) that the grains are clear and small in size, but when annealing at different temperatures (250, 350, 450, 550 and 650 $^{\circ}\text{C}$), they started to show an increase in clarity and homogeneity of the grain and even in the surface roughness also an increase in grain size which corresponds to the XRD results represented in Fig. 1. Furthermore, as can be seen in figure (4f) the crystal structure became more clear at 650 $^{\circ}\text{C}$.

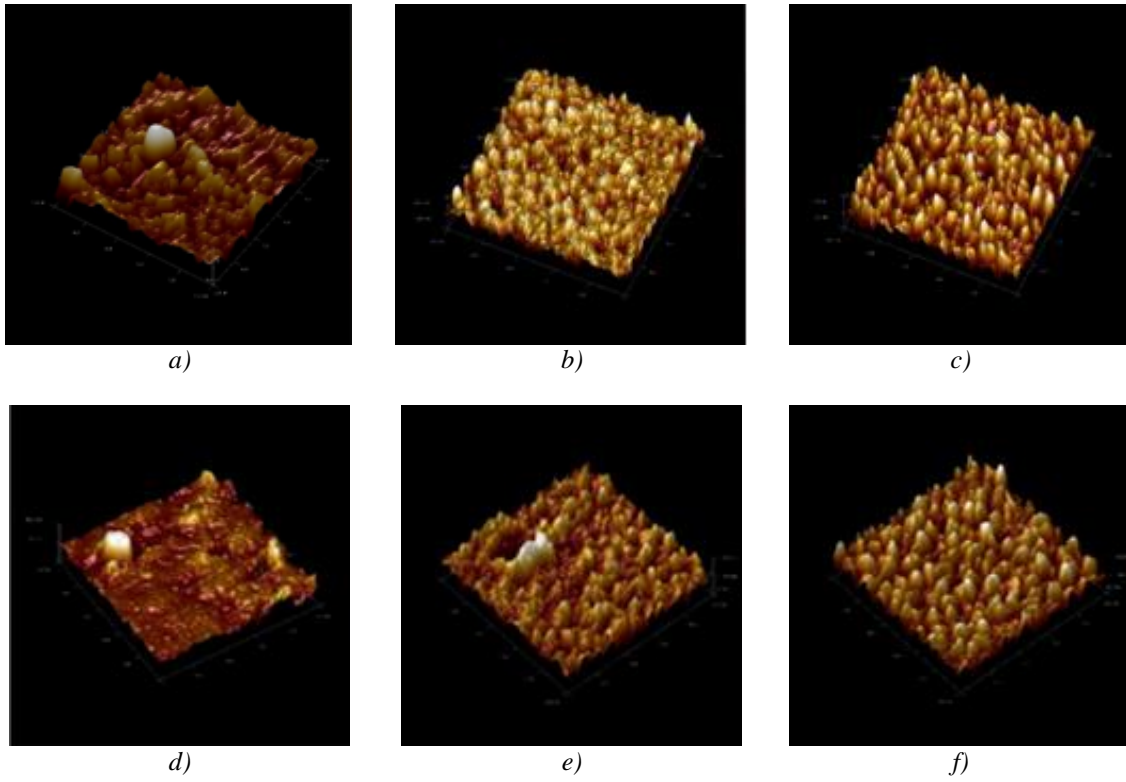


Fig. 3. AFM three-dimensional view of film morphology of ITO deposited on glass films. Five different annealed temperatures : (a) as-deposited (b).250 °C ,(c) 350 °C, (d) 450 °C ,(e) 550 °C and (f) 650 °C..

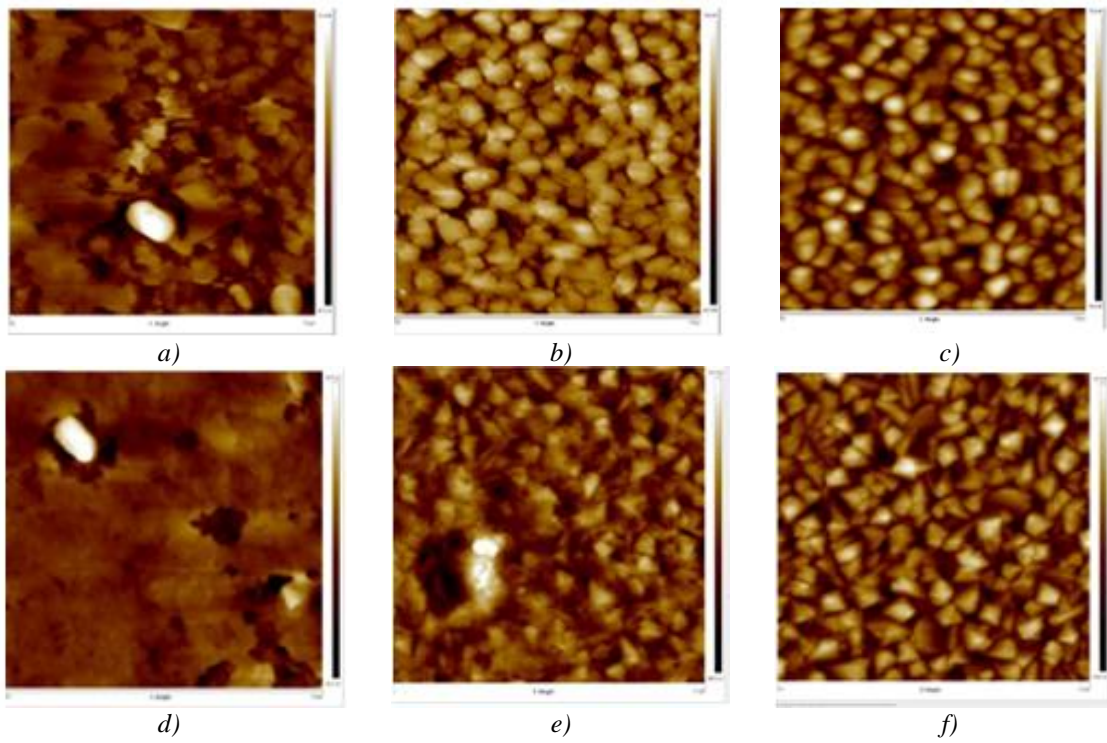


Fig. 4. AFM two-dimensional view of surface morphology of ITO deposited on glass films. Five different annealed temperatures :(a) as-deposited (b).250 °C ,(c) 350 °C, (d) 450 °C ,(e) 550 °C and (f) 650 °C

Some researchers represented that ITO films used as anode for OLEDs deposited at temperatures greater than 300 °C resulted in good performance of devices with high brightness [15-17]. Other researchers related the performance of OLED devices to the ITO surface morphology [17].

Table 4 represents the surface roughness at different annealing temperatures for ITO thin films.

Table 4. Roughness at different annealing temperatures for ITO thin films.

Temperature (°C)	Roughness (nm)
As – deposited	19.80
250	23.80
350	27.70
450	33.30
550	41.50
650	51.30

3.3. Effect of annealing on the optical properties of ITO films

The optical transmittance spectra of the as-deposited and annealed ITO grown by (Pulsed laser deposition PLD) on glass substrates are shown in Fig. 5. Transmissions of (≈ 80 -78%) in the near ultraviolet region (300nm) for 250, 450, 550 and 650 °C annealed are obtained, slightly lower than those for as-deposited ($\approx 88\%$), and slightly high than those for 350 °C annealed ($\approx 72\%$).

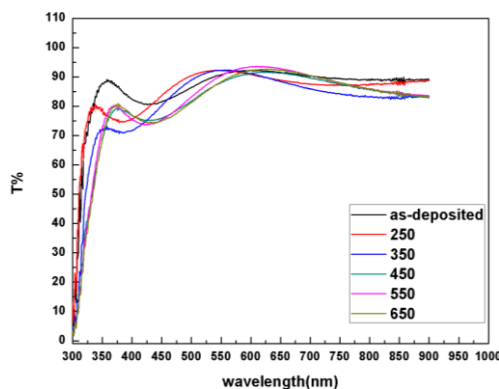


Fig. 5. Optical transmittance spectra of ITO thin films deposited on glass, annealed at 250, 350, 450, 550, and 650 °C.

Chauhan and co-authors reported that the (222) is the preferred orientation for the ITO films and exhibited high transmission up to 95% [18].

Fig. 6 showed the $(\alpha h\nu)^2$ as a function of $(h\nu)$ for the ITO films deposited on glass substrates at various annealing temperatures. The optical band-gap energy was found to decrease to 3.96 when the annealing temperature was increased to 450 °C.

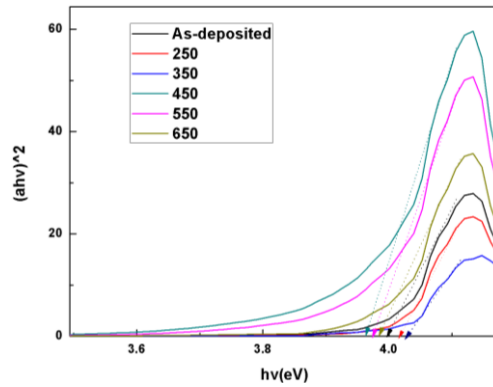


Fig. 6. $(\alpha h\nu)^2$ as function of $(h\nu)$ for ITO thin films deposited on glass, annealed at 250, 350, 450, 550, and 650 °C.

From Fig. 6, we get E_g by the extrapolation of the straight line to $(\alpha h\nu)^2 = 0$. The values of the energy gaps are displayed in Table 5.

Table 5. The band gap and transmissions of the as-deposited and annealed ITO thin films.

T (°C)	Transmissions(%)	Wavelength (nm)	Eg(eV)
As – deposited	88.40	321.27	3.99
250	79.50	319.34	4.01
350	79.03	320	4.03
450	79.18	328.58	3.96
550	78.38	326.5	3.97
650	80.30	322	3.98

A considerable decrease in Transmissions from 88% to 79% is found after annealing by 250 °C in the near ultraviolet region (300–400) nm as shown in Fig. 5. Meanwhile, a decrease in energy gap from 4.03eV to 3.96 eV is found between 350 °C and 450 °C as shown in Fig. 7.

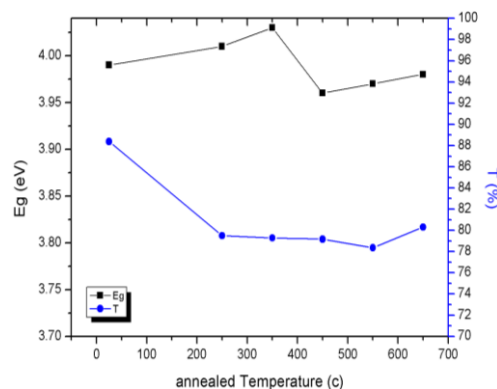


Fig. 7. Transmissions and Band gap energy of ITO change with Annealing Temperature\

3.4. Effect of annealing on the refractive index of ITO films

Fig. 8 represents the refractive index and extinction coefficient versus photon energy of the ITO thin films annealed at various temperatures. Table 6 represents the values of refractive index and extinction coefficient for the as-deposited and annealed ITO thin films.

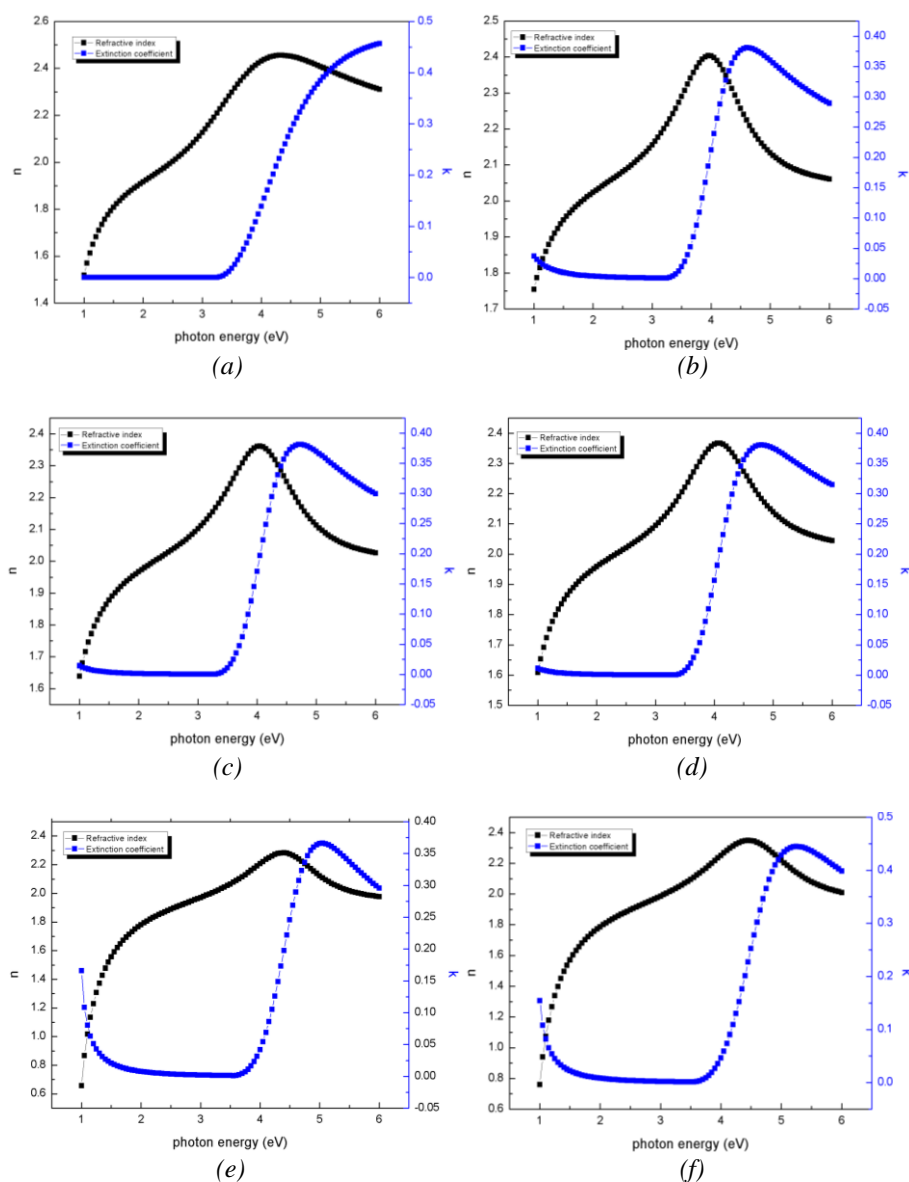


Fig. 8. Refractive index and Extinction coefficient of the ITO thin films annealed at: a) as deposited, b) 250°C, c) 350°C, d) 450°C, e) 550°C, f) 650°C

Table 6. Values of Refractive index and Extinction coefficient for the as-deposited and annealed ITO thin films.

T (°C)	Refractive index (n)	Extinction coefficient (k)
As – deposited	2.46	0.45
250	2.4	0.38
350	2.37	0.38
450	2.36	0.38
550	2.29	0.36
650	2.63	0.44

As shown in the Fig. 8 below, the samples of ITO thin films have almost the same refractive index in the measured photon energy range of 1-6 eV, also from measurement data in Table 6 we can say that the maximum value of refractive index ($n=2.63$) when the ITO film were annealed at 650°C . Regarding extinction coefficient, for annealing temperatures between 250 and 450°C , the ITO samples have almost the same value of extinction coefficient $k = 0.38$, from Table 6 the maximum value of extinction coefficient ($k=0.45$) for the as-deposited ITO thin films. The value of k decreases to 0.36 with increasing annealing temperature up to 550°C .

Tien and co-authors reported a refractive index between 2.01-2.04 and extinction coefficient $k = 5.6 \times 10^{-3} - 6.5 \times 10^{-3}$, for sputtered ITO, a transmission (T) between 85-87% at a wavelength of 500 nm and surface roughness between 2.64-2.74 nm [13].

4. Conclusions

The good optical and structural properties of ITO films deposited onto glass substrates indicate that the oxide films studied in this research are suitable as protective coatings and for opto-electronic devices such as anode for solar cells and light emitting diodes. Our results showed that the post-deposition annealing has an influence on the intensity of the diffraction peak and the film's structure. High values of optical transmittance were maintained at high annealing temperatures. Generally, the transmittance in the range 300–800 nm of all films on glass substrates slightly decreased with increasing annealing temperatures. Optical constants n and k increased by increasing the annealing temperature. Refractive index for the ITO films was reduced from 2.46 for as-deposited samples to 2.25 for samples annealed at 550°C . Also, the extinction coefficient decreases with annealing temperature up to 550°C .

AFM images for all samples showed an increase in the grain sizes and roughness of the films. Band gaps were reduced for the annealed samples which is a sign of improvement in the conductivity of the films. Further investigations may be necessary of the influence of post-deposition annealing on the thin film oxide properties.

Acknowledgements

The researchers acknowledge the Deanship of Scientific Research at Al Imam Mohammad Ibn Saud Islamic University, Saudi Arabia, for finance of this project.

References

- [1] J. H. Kim, K. A. Jeon, G. H. Kim, S. Y. Lee, Applied Surface Science **252**(13), 4834 (2006).
- [2] A. H. Sofi, M. A. Shah, K. Asokan, Journal of Electronic Materials **47**, 1344 (2018).
- [3] A. Al Yamani, N. Mustapha, Thin Solid Films **611**, 27 (2016).
- [4] T. Karasawa, Y. Miyata, Thin Solid Films **223**(1), 135 (1993).
- [5] M. J. Alam, D. C. Cameron, Thin Solid Films, **377–378**, 455 (2000).

- [6] U. Betz, M. K. Olsson, J. Marthy, M. Escolá, F. Atamny, *Surf. Coat. Technol.* **200**, 5751 (2006).
- [7] R. B. H. Tahar, T. Ban, Y. Ohya, Y. Takahashi, *J. Appl. Phys.* **83**, 2631 (1998).
- [8] T. P. Nguyena, P. Le Rendua, N. N. Dinha, M. Fourmigu, C. Meziere, *Synthetic Metals* **138**, 229 (2003).
- [9] Y. Cong, D. Han, J. Dong, S. Zhang, X. Zhang, Y. Wang, *Scientific Reports* **7**, 1497 (2017).
- [10] R. Riveros, E. Romero, G. Gordillo, *Brazilian Journal of Physics* **36**(3), 1042 (2006).
- [11] A. Rogozin, M. V. Vinnichenko, A. Kolitsch, W. Möller, *Journal of Vacuum Science & Technology A Vacuum Surfaces and Films* **22**(2), 349 (2004).
- [12] M. Nisha, S. Anusha, A. Anonym, M. Ramachandran, M. K. Jayaraj, *Applied Surface Science* **252**(5), 1430 (2005).
- [13] C.-L. Tien, *Advances in Condensed Matter Physics; New York* **2018**, (2018).
- [14] S. D'Elia, N. Scaramuzza, F. Ciuchi, C. Versace, G. Strangi, R. Bartolino, *Applied Surface Science* **255**, 7203 (2009).
- [15] E. Nam, Y.-H. Kang, D.-J. Son, D. Jung, S.-J. Hong, Y. S. Kim, *Surface and Coatings Technology* **205**(1), S129 (2010).
- [16] A. S. A. C. Diniza, C. J. Kiely, *Renewable Energy* **29**(13), 2037 (2004).
- [17] C. N. Li, C. Y. Kwong, A. B. Djurišić, P. T. Lai, P. C. Chui, W. K. Chan, S. Y. Liu, *Thin Solid Films* **477**(1-2), 57 (2005).
- [18] R. N. Chauhan, C. Singh, R. S. Anand, J. Kumar, *Journal of Nanotechnology* **2012**.